

A Clinician-Friendly Platform for Ophthalmic Image Analysis Without Technical Barriers

Meng Wang^{1,2#}, Tian Lin^{3,4#}, Qingshan Hou^{1,2,5#}, Aidi Lin^{3,4#}, Jingcheng Wang⁶, Qingsheng Peng⁷,
Truong X. Nguyen^{8,9}, Danqi Fang⁸, Ke Zou^{1,2}, Ting Xu^{1,2}, Cancan Xue⁷, Ten Cheer Quek⁷, Qinkai Yu¹⁰,
Minxin Liu^{1,2}, Hui Zhou¹¹, Zixuan Xiao¹², Guiqin He^{3,4,13}, Huiyu Liang¹⁴, Tingkun Shi^{3,4}, Man Chen^{3,4},
Linna Liu¹⁵, Yuanyuan Peng¹⁶, Lianyu Wang¹⁷, Qiuming Hu¹⁸, Junhong Chen¹⁹, Zhenhua Zhang²⁰,
Cheng Chen²¹, Yitian Zhao²², Dianbo Liu¹⁷, Jianhua Wu¹⁵, Xinjian Chen²³, Changqing Zhang²⁴,
Triet Thanh Nguyen⁹, Yanda Meng^{10,25}, Yalin Zheng^{25,26}, Yih Chung Tham^{1,2}, Carol Y. Cheung⁸,
Huazhu Fu^{27(✉)}, Haoyu Chen^{3,4,8(✉)}, and Ching-Yu Cheng^{1,2,7,28(✉)}

- ¹ Centre for Innovation and Precision Eye Health, Yong Loo Lin School of Medicine, National University of Singapore, Singapore 119228, Singapore.
- ² Department of Ophthalmology, Yong Loo Lin School of Medicine, National University of Singapore, Singapore 119228, Singapore.
- ³ Joint Shantou International Eye Center, Shantou University and the Chinese University of Hong Kong, 515041 Shantou, Guangdong, China.
- ⁴ Shantou University Medical College, 515041 Shantou, Guangdong, China.
- ⁵ School of Computer Science and Engineering, Northeastern University, 110819 Shenyang, Liaoning, China.
- ⁶ Big Vision Medical Technology Ltd., 215011 Suzhou, China.
- ⁷ Singapore Eye Research Institute, Singapore National Eye Centre, Singapore 169856, Singapore.
- ⁸ Department of Ophthalmology and Visual Sciences, The Chinese University of Hong Kong, 999077 Hong Kong Special Administrative Region, China.
- ⁹ Binh Dinh Eye Hospital, Vietnam.
- ¹⁰ Department of Computer Science, University of Exeter, Exeter, EX4 4RN, UK.
- ¹¹ University of Science and Technology Hospital, 518000 Shenzhen, Guangdong, China.
- ¹² Shenzhen Qianhai Shekou Free Trade Zone Hospital, 518000 Shenzhen, Guangdong, China.
- ¹³ Department of Ophthalmology, Meizhou People's Hospital, Meizhou Academy of Medical Sciences, 514000 Meizhou, Guangdong, China.
- ¹⁴ Department of Ophthalmology, Yeungnam University College of Medicine, 42417 Daegu, South Korea.
- ¹⁵ Aier Eye Hospital of Wuhan University, 430000 Wuhan, Hubei, China.
- ¹⁶ School of Biomedical Engineering, Anhui Medical University, 230032 Hefei, Anhui, China.
- ¹⁷ College of Computer Science and Technology, Nanjing University of Aeronautics and Astronautics, 211100 Nanjing, Jiangsu, China.
- ¹⁸ Guangxi Jingliang Eye Hospital, 530021 Nanning, Guangxi, China.
- ¹⁹ Puning People's Hospital, 522000 Jieyang, Guangdong, China.
- ²⁰ Qingdao Central Hospital, University of Health and Rehabilitation Sciences (Qingdao Central Hospital), 266042 Qingdao, Shandong, China.
- ²¹ Department of Electrical and Electronic Engineering, the University of Hong Kong, Hong Kong, China.
- ²² Ningbo Institute of Materials Technology and Engineering, Chinese Academy of Sciences, 315201 Ningbo, Zhejiang, China.
- ²³ School of Electronics and Information Engineering, Soochow University, 215006 Suzhou, Jiangsu, China.
- ²⁴ College of Intelligence and Computing, Tianjin University, 300350 Tianjin, China.
- ²⁵ Liverpool Centre for Cardiovascular Science, University of Liverpool and Liverpool Heart and Chest Hospital, Liverpool, United Kingdom.
- ²⁶ Department of Eye and Vision Sciences, University of Liverpool, Liverpool, United Kingdom.
- ²⁷ Institute of High Performance Computing (IHPC), Agency for Science, Technology and Research (A*STAR), Singapore 138632, Singapore.
- ²⁸ Ophthalmology & Visual Sciences Academic Clinical Program (EYE ACP), Duke-NUS Medical School, Singapore 169856, Singapore.

M. Wang, T. Lin, Q. Hou, and A. Lin are the co-first authors.

✉ H. Fu, H. Chen, and C.-Y. Cheng are the co-corresponding authors and contributed equally.

Abstract. Artificial intelligence (AI) shows remarkable potential in medical imaging diagnostics, yet most current models require retraining when applied across different clinical settings, limiting their scalability. We introduce GlobeReady, a clinician-friendly AI platform that enables fundus disease diagnosis that operates without retraining, fine-tuning, or the needs for technical expertise. GlobeReady demonstrates high accuracy across imaging modalities: 93.9–98.5% for 11 fundus diseases using color fundus photographs (CFPs) and 87.2–92.7% for 15 fundus diseases using optic coherence tomography (OCT) scans. By leveraging training-free local feature augmentation, GlobeReady platform effectively mitigates domain shifts across centers and populations, achieving accuracies of 88.9–97.4% across five centers on average in China, 86.3–96.9% in Vietnam, and 73.4–91.0% in Singapore, and 90.2–98.9% in the UK. Incorporating a built-in confidence-quantifiable diagnostic mechanism further enhances the platform’s accuracy to 94.9–99.4% with CFPs and 88.2–96.2% with OCT, while enabling identification of out-of-distribution cases with 86.3% accuracy across 49 common and rare fundus diseases using CFPs, and 90.6% accuracy across 13 diseases using OCT. Clinicians from countries rated GlobeReady highly for usability and clinical relevance (average score 4.6/5). These findings demonstrate GlobeReady’s robustness, generalizability and potential to support global ophthalmic care without technical barriers.

1 Introduction

Diseases of retinal and optic nerve head, such as diabetic retinopathy (DR), age-related macular degeneration (AMD), and glaucoma, represent the leading cause of visual impairment and blindness globally, affecting hundreds of millions and imposing significant burdens on healthcare systems [1, 2]. Early detection and accurate diagnosis are essential for effective treatment and the prevention of irreversible vision loss [3]. Color fundus photography (CFP) and optical coherence tomography (OCT) are critical imaging tools in ophthalmic practice, playing a key role in supporting clinical diagnosis.

Artificial intelligence (AI) has significantly advanced medical imaging analysis^{4,5}, particularly in disease diagnosis [4, 5], particularly in disease diagnosis [6, 7]. Although AI models have demonstrated impressive performance in diagnosing ocular diseases, the majority of them focus narrowly on specific diagnostic tasks, limiting their generalizability to broader and more complex clinical scenarios. Recently, ophthalmic foundation models such as RETFound [8] and VisionFM [9] have emerged. Trained on extensive unannotated ophthalmic image datasets via self-supervised learning, these models showed promising performance across a range of downstream tasks.

Nevertheless, adapting foundation models to specific clinical contexts typically requires retraining or fine-tuning to accommodate varying diseases or feature distributions. This adaptation demands substantial computational resources and expertise in AI model development, posing significant barriers for clinicians who lack specialized expertise in AI and programming [10]. Consequently, clinicians seeking to train and apply AI models to specific diagnostic tasks often face the need to transfer locally acquired data to developers for model training, retraining or fine-tuning, leading to delays and inefficiencies [11, 12]. Furthermore, strict institutional data-sharing policies and administrative hurdles rooted in privacy and security concerns pose significant barriers to AI adoption in the clinical environment. Additionally, existing AI models often focus on a limited range of disease categories, which can lead to poor performance when encountering unseen, out-of-distribution (OOD) diseases. Such performance gaps may result in misdiagnosis or overlooked conditions, adversely impacting patient outcomes. In another scenario, for the uncommon diseases, clinicians often need to refer to specific cases from extensive literature or conduct a detailed image search before making a diagnosis; however, an automatic tool to facilitate this process has not yet been developed.

In this study, we developed GlobeReady, a clinician-friendly ophthalmic image analysis platform that enables clinicians to seamlessly perform ocular disease diagnosis, generate confidence-quantifiable ocular disease predictions, and retrieve cases based on specific features. Fig. 1 illustrates an overview of GlobeReady’s architecture and application workflow. We collected 488,448 ophthalmic images, including 382,527 CFPs and 105,921 OCT images from open datasets, ophthalmic literature, and online resources, representing a wide range of diseases across various ethnicities and regions around the world. Furthermore, leveraging these globally sourced datasets, we first synthesized 38 million ophthalmic images using a generative model to create a large-scale synthetic dataset. We then curated 475,845 real image-text pairs from these global datasets. We then curated 475,845 real image-text pairs from these global datasets. We first employed the self-supervised pretraining framework DINOv2 [13] on the synthetic dataset, allowing the model to capture detailed ophthalmic image features and structural information. We then conducted further pretraining using the contrastive learning framework CLIP [14] on the curated 475,845 image-text pairs, aligning visual features with semantic context to enhance complex feature representation. These advanced pretraining techniques enable GlobeReady to offer an innovative clinician-friendly platform that is entirely code- and training-free, streamlining the use of AI in clinical practice.

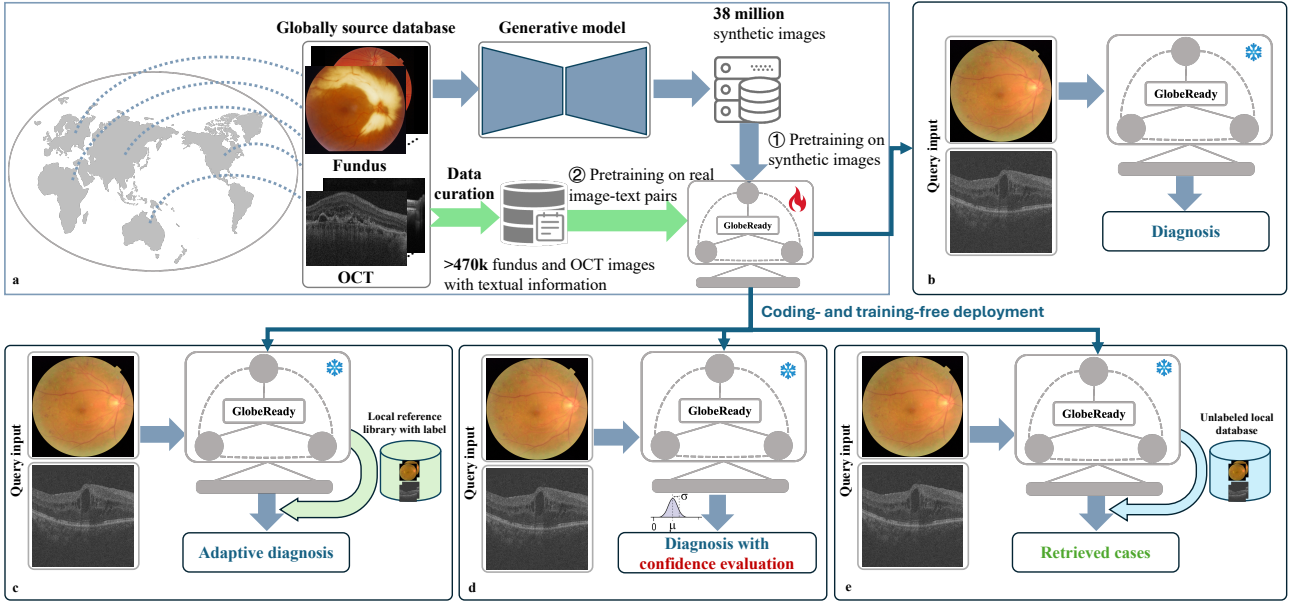


Figure 1. Overview of the GlobeReady. a, Data collection and model pre-training; b, GlobeReady disease diagnosis; c, Adaptive ocular disease diagnosis with local retrieval augmentation; d, Confidence-quantifiable ocular disease diagnosis; e, Feature-based case retrieval.

2 Results

2.1 Ocular disease diagnosis by GlobaFree

With GlobeReady’s built-in ocular disease diagnosis feature (Fig. 1b), GlobeReady demonstrated exceptional performance across multiple datasets involving diverse disease categories and imaging modalities. Specifically, it achieved a Top-1 accuracy of 93.9% and Top-1 recall of 91.6% on a dataset comprising 7,808 CFPs covering 11 disease categories from 5 hospitals in China (termed as JLHW11 dataset; Fig. 2a, Supplementary Fig. 1a), which includes CFPs of 10 retinal disorders and normal conditions (Supplementary Table 1). Additionally, our model achieved Top-3 and Top-5 accuracies of 97.6% and 98.5%, respectively, with corresponding recalls of 96.0% and 97.3%. Notably, the Top-5 recall ranged from 88.2% to 99.9% across all conditions (Supplementary Table 1), including macular, optic nerve head-related, retinal vascular, and other retinal diseases.

We further evaluated GlobeReady’s diagnostic performance using an OCT dataset curated by the Joint Shantou International Eye Center spanning 15 types of ocular conditions (JSIEC-OCT15 dataset; Fig. 2b, Supplementary Fig. 1b; Supplementary Table 2). The model demonstrated promising results, achieving Top-1, Top-3, and Top-5 accuracies of 87.2%, 90.9%, and 92.7%, respectively. The corresponding average recall rates were 86.3%, 89.8%, and 91.7%, with the Top-5 recall ranging from 71.8% to 99.5% across all 15 conditions.

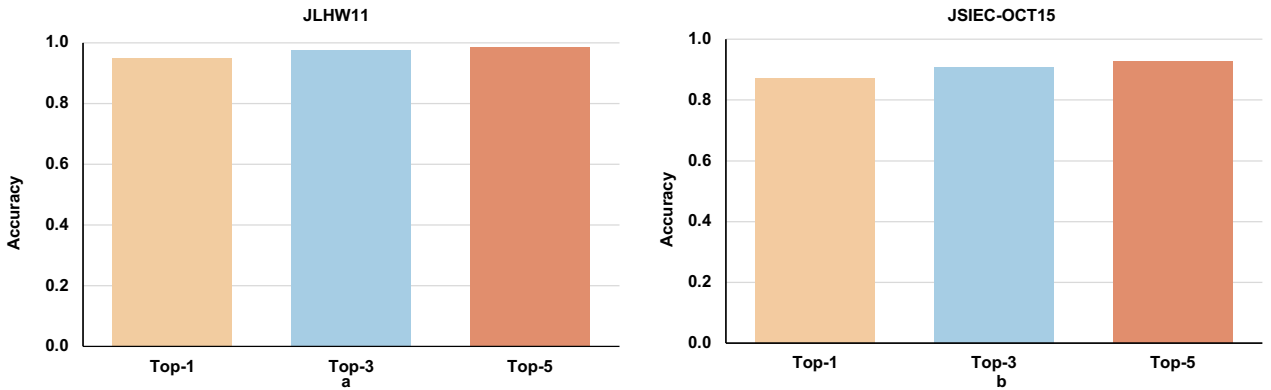


Figure 2. Performance of GlobeReady for identifying ocular diseases on different datasets. JLHW11 is a CFP dataset from the Joint Shantou International Eye Center (JSIEC), Longchuan People’s Hospital, Haifeng Pengpai Memorial Hospital, and Wuhan Aier Eye Hospital (WAEH), covering 11 categories. JSIEC-OCT15 is an OCT dataset created by Joint Shantou International Eye Center with 15 categories.

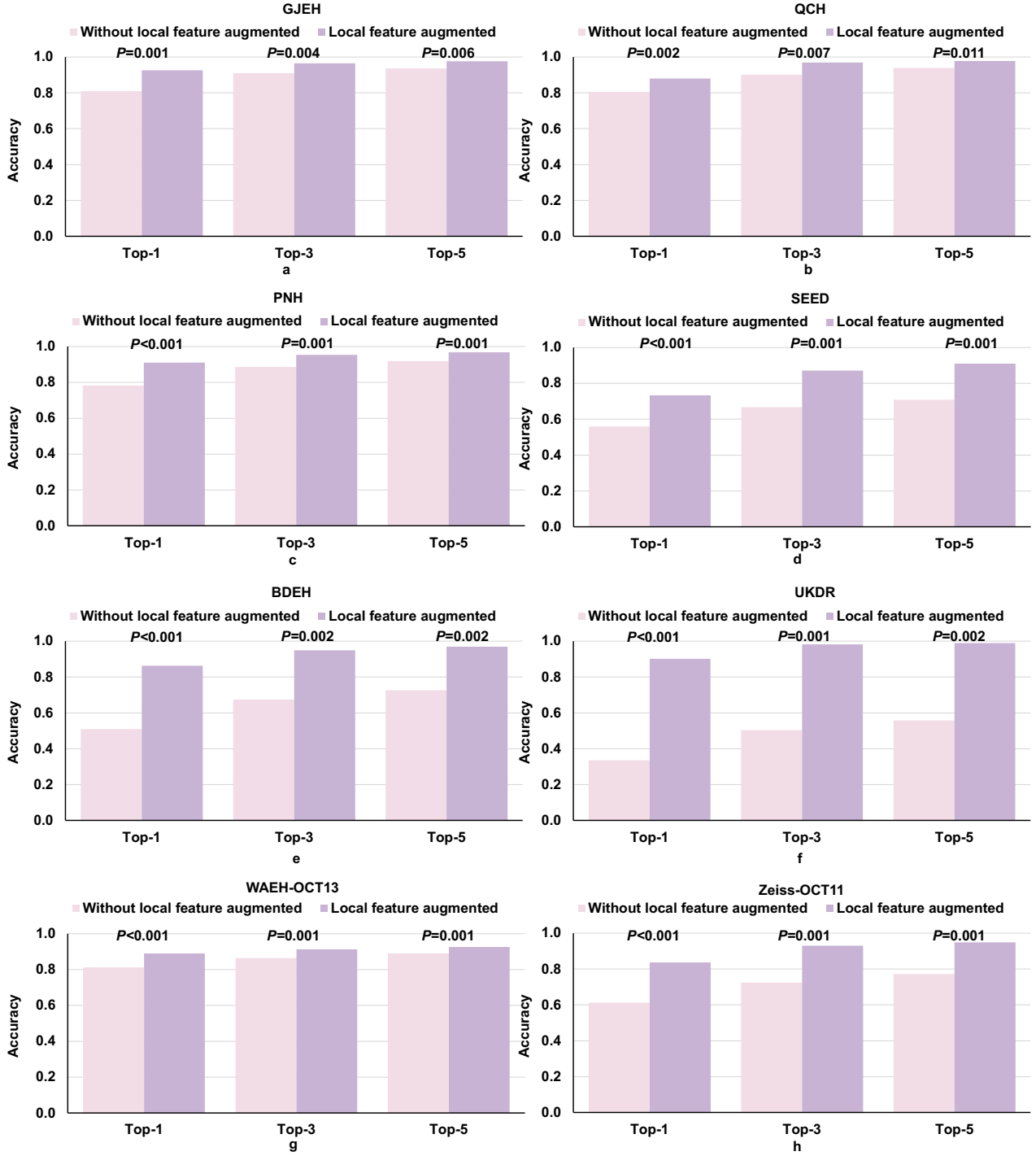


Figure 3. Results of local retrieval augmented ocular disease diagnosis and confidence-quantifiable ocular disease diagnosis. a, The Guangxi Jingliang Eye Hospital (GJEH) dataset includes the same disease categories as JLHW11; b, QCH dataset, from Qingdao Central Hospital, comprises images labeled as normal, AMD, DR, and glaucoma. c, PNH dataset, from Puning People’s Hospital, also shares the same categories as JLHW11. d, The Singapore Epidemiology of Eye Diseases (SEED) dataset, collected in Singapore, includes annotations for diagnosing AMD, DR, and glaucoma. e, BDEH dataset originates from Binh Dinh Eye Hospital in Vietnam. f, UKDR dataset, was collected from a DR screening program in the University of Liverpool, the United Kingdom. g, WAEH-OCT13 dataset is a local OCT dataset from the Wuhan Aier Eye Hospital. h, The Zeiss-OCT11 dataset is a local OCT dataset acquired by the device of Zeiss.

2.2 Adaptive ocular disease diagnosis by local retrieval augmented GlobeReady

AI models often necessitate retraining to adapt to varying tasks or domains, such as different clinics or geographical regions, due to variations in equipment, ethnicity, and disease prevalence. Drawing inspiration from retrieval augmented generation (RAG) techniques in large language models (LLMs) [15, 16], GlobeReady addresses this challenge by enhancing the base reference features with locally extracted data, eliminating the need for retraining (Fig. 1c). We used features extracted from the reference subset of the JLHW11 dataset from China as the CFP base reference feature library and used diverse external datasets through local retrieval augmented approach to improve the model diagnostic performance. As shown in Figure 3, , in all the participating centers, diagnostic performance across all participating centers improved when local features were augmented, compared to when they were not, particularly in the centers outside China (Supplementary Fig. 2, and Supplementary Table 3-7). We further evaluated GlobeReady’s performance across three clinical centers in different countries. At the Singapore Eye Research Institute, its performance gains across multi-ethnic populations in the Singapore Epidemiology of Eye Diseases (SEED) Study36, with Top-1 to Top-5 accuracies improved by 28.3-31.1%, reaching to 73.4-91.0% ($P \leq 0.001$ compared to before local retrieval augmentation; Fig.3d, Supplementary Fig. 2d, Supplementary Table 6). At Binh Dinh Eye Hospital in Vietnam, accuracies rose from 51.0–72.7% to 86.3–96.9% ($P \leq 0.002$), with similar gains observed in recall scores (Fig.3e, Supplementary Fig. 2e, Supplementary Table 7). Likewise, at the Department of Eye and Vision Sciences, University of Liverpool in the United Kingdom, GlobeReady’s diagnostic performance improved significantly by 76.9-168.5% following local feature augmentation, with accuracies rising from 33.6-55.9% to 90.2-98.9% ($P \leq 0.002$, Fig. 3f, Supplementary Fig. 2f, and Supplementary Table 7) for CPFs collected from a diabetic retinopathy (DR) screening program (referred as UKDR dataset thereafter).

We further evaluated GlobeReady’s performance in identifying ocular diseases in OCT images with local retrieval augmented diagnosis, using features from the reference subset of JSIEC-OCT15 as the base OCT reference feature library. In the WAEH-OCT13 dataset, which encompasses 12 ocular diseases along with normal conditions, Top-1, Top-3, and Top-5 accuracies increased from ranges of 81.2–89.0% to 89.0–92.5% ($P \leq 0.001$), with recall rates improving to 86.6–91.3% (Fig. 3g, Supplementary Fig. 2g, Supplementary Table 9). Similarly, in the Zeiss-OCT11 dataset, accuracies rose from 61.3–77.2% to 83.7–94.9% ($P \leq 0.001$) following the augmentation of local features, accompanied by comparable improvements in recall rates (Fig. 3h, Supplementary Fig. 2h, Supplementary Table 10).

2.3 Confidence-quantifiable ocular disease diagnosis with Bayesian GlobeReady

Providing diagnostic results with a reliability assessment is crucial for deploying AI models in clinical practice. Therefore, we integrated Bayesian uncertainty evaluation into our GlobeReady platform (Fig. 1d). This feature improved GlobeReady’s performance on the JLHW11 dataset, increasing Top-1 accuracy from 93.9% to 94.9% ($P = 0.001$) and Top-1 recall rates from 91.6% to 92.1% with $P = 0.007$ (Fig. 4a, Supplementary Table 11). Similar improvements were noted in the JSIEC-OCT15 dataset, with Top-1 accuracy rising from 87.2% to 88.2% ($P < 0.001$) and recall reaching 87.0% with $P < 0.001$ (Fig. 4b, Supplementary Table 12).

Furthermore, implementing a confidence threshold to flag cases for further clinical review would reduce misdiagnosis risk. Post-flagging, GlobeReady’s Top-1 accuracy and recall rates on the JLHW11 dataset improved to 99.4% and 98.5% ($P = 0.001$), respectively, with recall rates across categories ranging from 91.2% to 100%. For OCT images, similar strategies enhanced Top-1 accuracy to 96.2% and recall to 94.5% on the JSIEC-OCT15 dataset ($P > 0.001$).

We fine-tuned two other foundation models, RETFound [8] and VisionFM [9], and then compared their diagnostic performance with our GlobeReady. GlobeReady showed superior performance in Top-3, Top-5, and confidence-thresholded accuracy and recall rates without fine-tuning ($P \leq 0.001$), and achieved comparable or superior Top-1 across both JLHW11 and JSIEC-OCT15 datasets (Supplementary Fig. 3).

2.4 Open set anomaly detection with Bayesian GlobaFree

To assess GlobeReady’s reliability in real-world clinical settings where patients may present with previously unseen conditions, we constructed a new evaluation dataset (termed CFPOOD49), containing 7,257 fundus images across 49 disease categories not included in the original JLHW11 reference set (Fig. 5a). Using features from the JLHW11 reference subset as the base CFP feature library, GlobeReady accurately flagged the samples in the CFPOOD49 dataset, achieving detection rates ranging from 66.7% to 100.0%. Several conditions, including choroidal osteoma and multiple evanescent white-dot syndromes, reached perfect detection (100%). Most diseases showed strong detection rates (85–95%), while a few, such as Purtscher retinopathy, were lower due to small sample sizes. Notably, epiretinal membrane, the largest class with 2,097 images, achieved 90.2%. Additionally, GlobeReady demonstrated robust performance on a separate dataset of 1,066 low-quality fundus images, reaching a 94.6% detection rate using a confidence threshold strategy.

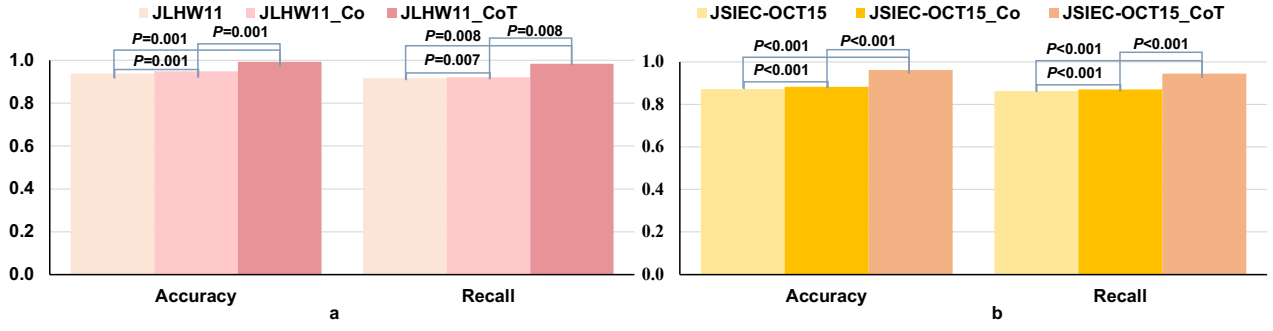


Figure: 4. Confidence-quantifiable ocular disease diagnosis. JLHW11 and JSIEC-OCT15 represent the GlobeReady’s performance without introducing confidence-quantification; JLHW11_Co and JSIEC-OCT15_Co indicate the GlobeReady’s performance with confidence-quantification; JLHW11_CoT and JSIEC-OCT15_CoT are the performance of GlobeReady after implementing a confidence threshold recommendation. In this last scenario, samples exhibiting low confidence are flagged for re-evaluation by a clinician.

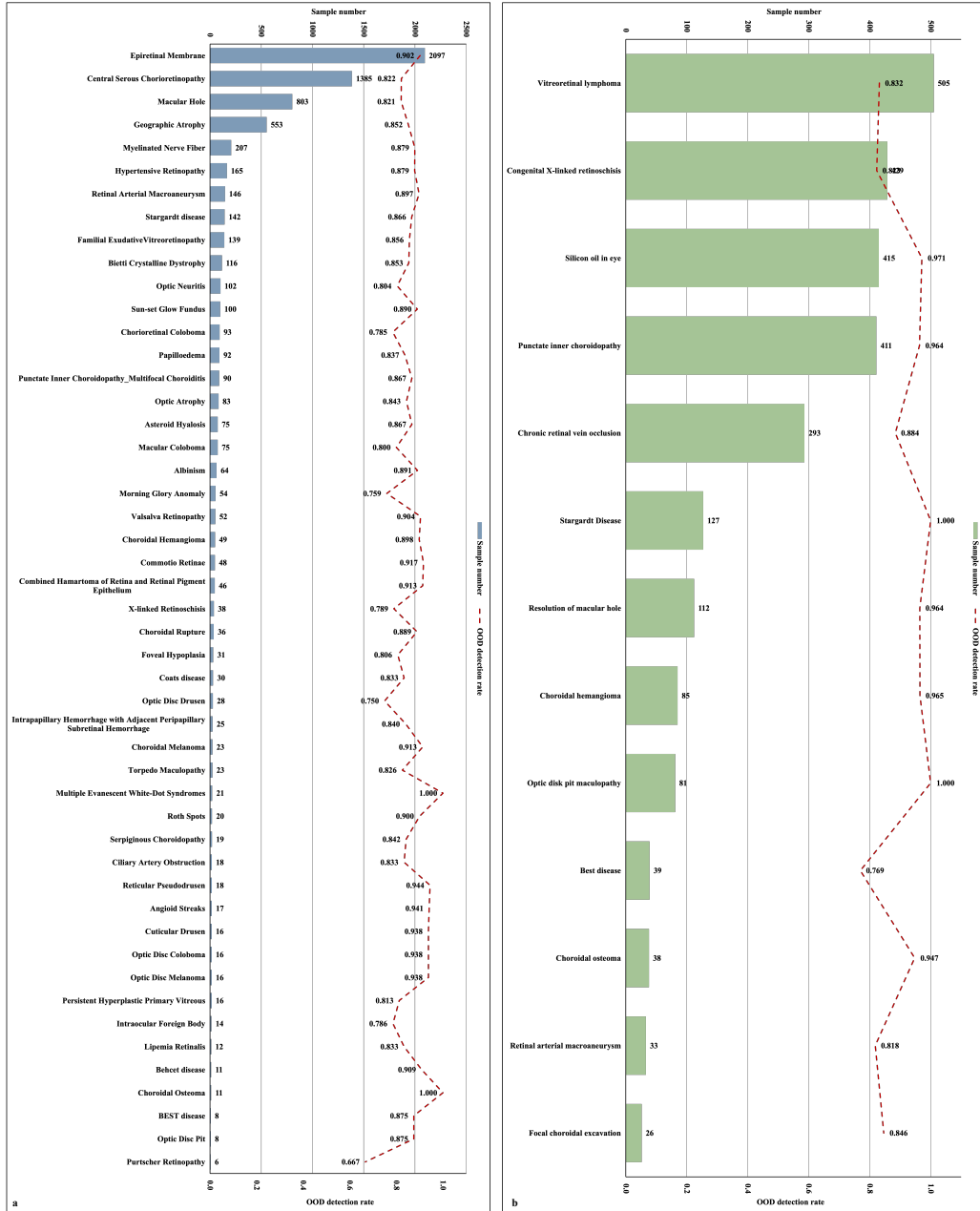


Figure: 5. GlobeReady’s performance in detecting out-of-distribution (OOD) fundus diseases in an open-set scenario. a, Data distribution and corresponding OOD detection rates for the 49 disease categories in CFPOOD49 dataset. b, Data distribution and corresponding OOD detection rates for the 13 disease categories in OCT-OOD13 dataset.

We further validated GlobeReady’s ability to detect unfamiliar disease categories in OCT images. A new evaluation dataset, OCT-OOD13, was curated, comprising 2,594 OCT scans across 13 disease categories not present in the JSIEC-OCT15 reference set (Fig. 5b). Using features from JSIEC-OCT15 as the base OCT feature library, GlobeReady flagged most samples with unseen conditions from OCT-OOD13 dataset, achieving detection rates ranging from 66.7% to 100.0%. Perfect detection was observed for Stargardt disease and optic disc pit maculopathy (100.0%), while conditions such as silicone oil-filled eyes, punctate inner choroidopathy, and choroidal hemangioma also achieved high detection rates ($>94\%$). Moderate-to-high performance was observed for chronic retinal vein occlusion, focal choroidal excavation, and vitreoretinal lymphoma (83–88%), demonstrating GlobeReady’s strong generalizability across diverse OCT abnormalities. To further assess robustness against image quality degradation, we tested the model on 2,016 low-quality OCT scans, achieving a 92.8% detection rate using confidence-threshold filtering.

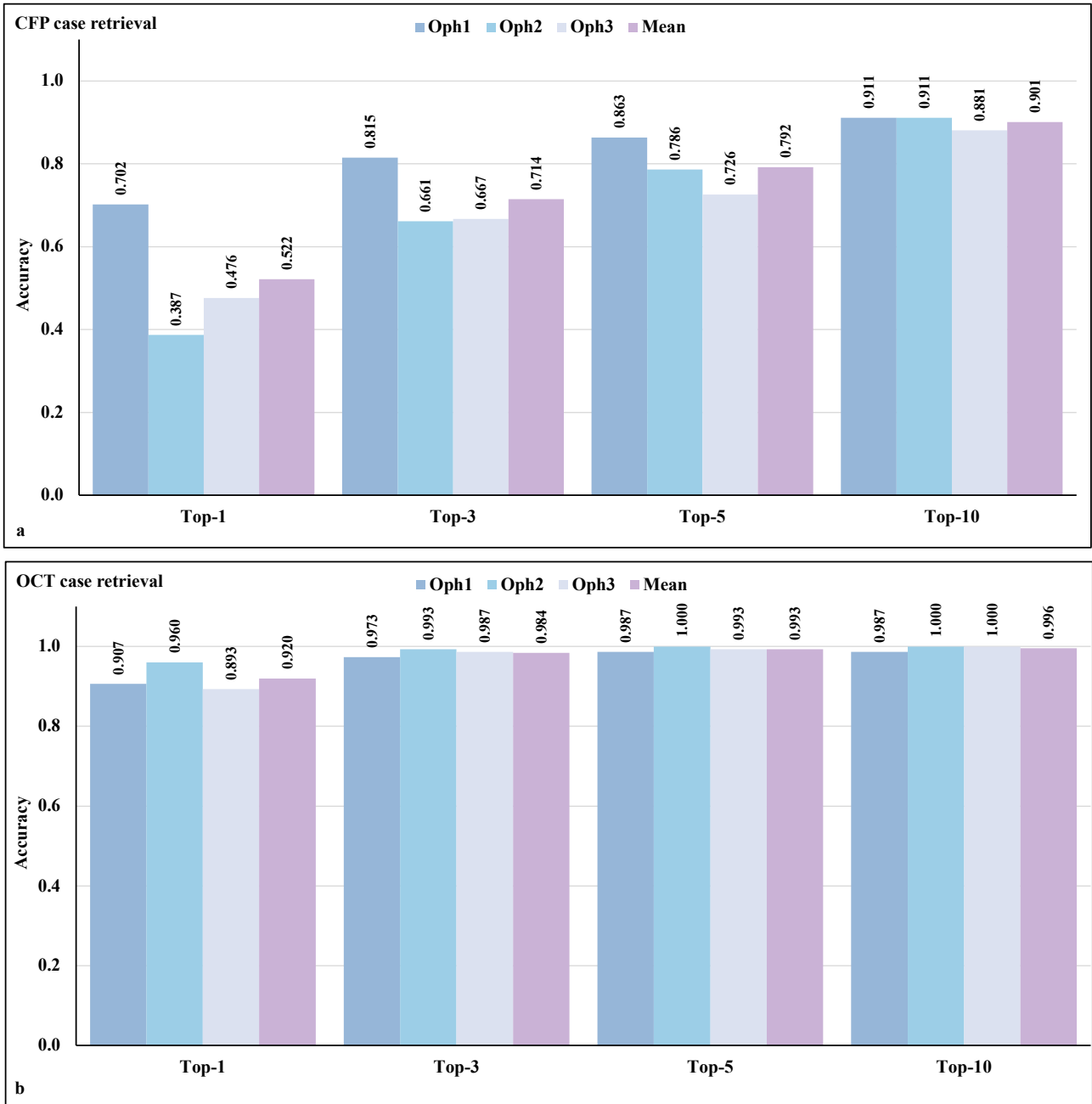


Figure 6. Top-k score in prospective evaluation of feature-based case retrieval. a, The prospective evaluation results of feature-based case retrieval for CFPs; b, The prospective evaluation results of feature-based case retrieval for OCT images. Doctor1, Doctor2, and Doctor3 refer to the three ophthalmologists who participated in the prospective evaluation.

Table: 1. Questionnaire results for GlobeReady.

Sections		Scores (Mean \pm SD)
System usability scale*		86.4 \pm 14.4
Question 1	I think that I would like to use this system frequently.	3.3 \pm 0.8
Question 2	I found that system unnecessarily complex.	3.6 \pm 0.5
Question 3	I thought the system was easy to use.	3.4 \pm 0.8
Question 4	I think that I would need the support of a technical person to be able to use this system.	3.1 \pm 1.2
Question 5	I found that the various functions in this system were well integrated.	3.4 \pm 0.5
Question 6	I thought that there was too much inconsistency in this system.	3.6 \pm 0.5
Question 7	I would imagine that most people would learn to use this product very frequently.	3.4 \pm 0.5
Question 8	I found the system very awkward to use.	3.6 \pm 0.5
Question 9	I felt very confident using the system.	3.6 \pm 0.5
Question 10	I needed to learn a lot of things before I could get going with this system.	3.6 \pm 0.5
Effectiveness		4.3 \pm 0.4
Question 1	I spend less time in clinical diagnosis by utilizing the system.	4.3 \pm 0.5
Question 2	The results generated by the system are trustworthy and accurate.	4.4 \pm 0.5
Question 3	It would cost me more time to read and correct the diagnosis results.	4.3 \pm 0.8
Helpfulness		4.6 \pm 0.5
Question 1	The system can assist me in clinical diagnosis.	4.7 \pm 0.5
Question 2	The uncertainty provided by the system is helpful.	4.6 \pm 0.5
Ease of use		4.7 \pm 0.5
Question 1	The user interface is clear and easy to understand.	4.7 \pm 0.5
Question 2	I find it difficult to use the system as its guidance is unclear.	4.7 \pm 0.5
Satisfaction		4.6 \pm 0.4
Question 1	I would like to recommend my colleagues to use this system.	4.4 \pm 0.5
Question 2	I would use this system in my future work.	4.7 \pm 0.5

*System usability scale score was calculated by multiplying the score for each question (Questions 1 to 10) by 2.5, and the max score for each question is 4.

2.5 Feature-based case retrieval with GlobeReady

GlobeReady facilitates rapid retrieval of similar cases without the need for retraining (Fig. 1e). We assessed its performance using an additional set of 168 CFPs, across 12 ophthalmic diseases, collected from Vietnam, Supplementary Fig. 4a) to retrieve similar cases from the JLHW11 and CFPOOD49 datasets). Retrieval performance varied across diseases, with Top-1 to Top-10 recall rates differing by condition (Supplementary Fig. 4b). The highest Top-1 recall was observed for epiretinal membrane (0.968), followed by sunset-glow fundus (0.889). Central serous chorioretinopathy and hypertensive retinopathy achieved 0.795 and 0.750, respectively. Rare conditions such as macular coloboma and optic neuritis initially showed poor Top-1 recall rate, but improved to 1.0 when considering Top-3 or Top-10 results.

To evaluate GlobeReady clinically, we conducted a retrieval study using these 168 CFPs as queries against a large-scale reference database (CFP700K) containing 747,237 unlabeled CFPs sourced from multiple hospitals and diverse imaging devices. GlobeReady returned the Top-10 most similar images per query, yielding 1,680 retrieved images. These were reviewed by three experienced ophthalmologists via an online platform we developed (Supplementary Fig. 5). The assessments showed average accuracy rates of 0.522 for Top-1, 0.714 for Top-3, 0.792 for Top-5, and 0.901 for Top-10, demonstrating GlobeReady’s high reliability in retrieving clinically relevant cases (Fig. 6a), especially when multiple top results are considered. Additionally, GlobeReady’s OCT retrieval performance was tested using 150 OCT images from JSIEC as queries against 34,384 unlabeled OCT scans from Wuhan Aier Eye Hospital. The retrieval results, assessed by three ophthalmologists via our platform (Supplementary Fig. 6), showed efficient and accurate retrieval of highly similar OCT cases without model retraining (Fig. 6b). The average Top-1 accuracy was 0.920, closely aligning with clinical judgment, and improved to 0.984 for Top-3, 0.993 for Top-5, and 0.996 for Top-10.

2.6 Questionnaire evaluations for GlobeReady platform

To evaluate the usability and acceptability of the GlobeReady platform, seven ophthalmologists from China and Singapore were asked to complete a questionnaire after using the platform. The questionnaire consisted of the system usability scale (SUS) [17], effectiveness, helpfulness, ease of use, and satisfaction (Supplementary Questionnaire). Among the seven participating clinicians, three (42.9%) used both fundus and OCT images, three (42.9%) used only fundus images, and one (14.2%) used only OCT images. Regarding the intended use scenarios of the platform, six participants (85.7%) reported using it for labelling images, three (42.9%) indicated its use for daily clinical diagnosis, and three (42.9%) would use it for clinical teaching. The results of the survey showed that GlobeReady obtained an average SUS score of 86.4 \pm 14.4, indicating a level of “excellent” usability [18]. For the questions in other sections, a 5-point Likert scale was used (1-5). The average Likert

scores were 4.3 ± 0.4 for effectiveness, 4.6 ± 0.5 for helpfulness, 4.7 ± 0.5 for ease of use, 4.6 ± 0.4 for satisfaction, respectively (Table 1). Specifically, the participating clinicians reported that the GlobeReady platform could reduce time spent on making clinical diagnosis, with an average Likert score of 4.3 ± 0.5 , and the generated diagnostic results were accurate and trustworthy, with an average Likert score of 4.4 ± 0.5 . While it would take some time to generate the results by the platform, most of the clinicians did not feel this was time-consuming (converted Likert score = 4.3 ± 0.8). In addition to efficiency, the clinicians also found the uncertainty evaluation helpful, with an average Likert score of 4.6 ± 0.5 . Moreover, majority of them agreed that the GlobeReady platform’s interface was clear and understandable (Likert score = 4.7 ± 0.5), and they would like to use it in future work (Likert score = 4.7 ± 0.5).

2.7 Model interpretation

To investigate the attribution patterns of GlobeReady’s pretrained weights, without task-specific retraining, across ocular imaging modalities, we employed AGFVisualization [19], a saliency mapping technique. Our analysis revealed that GlobeReady intrinsically localized disease-specific features in CFPs, such as macular area for AMD, optic disc for glaucoma, and retinal vascular abnormalities for branched retinal vascular occlusion (Supplementary Fig. 7). Similarly, OCT analysis demonstrated precise attention to pathological structures across retinal layers Supplementary Fig. 8). These visualization results provided mechanistic evidence for GlobeReady’s robust feature-matching performance, showing that its pretrained representations inherently capture clinically relevant pathological areas spanning multiple ocular disease categories and imaging modalities.

3 Discussion

We present GlobeReady, a clinician-friendly AI platform that enables direct deployment without requiring coding expertise or model retraining. This represents a fundamental departure from conventional diagnostic AI systems, which face clinical adoption barriers due to specialized programming requirements and the need for clinic-specific retraining. By integrating DINOv2 [13] with a CLIP-based pretraining framework [14] GlobeReady acquires robust and generalizable feature representations that enable immediate clinical applicability while maintaining diagnostic performance-resolving the critical accessibility-versus-accuracy trade-off that has limited real-world implementation of AI models.

Compared to previous coding-free platforms [20, 21] and proprietary solutions like Google AutoML [22] and Microsoft Azure ML Studio [23], GlobeReady stands out through its feature matching-based diagnostic approach, which transcends the need for retraining by utilizing a comprehensive, pre-curated feature library. This design not only accelerates adaptation across diverse ophthalmic imaging modalities but also minimizes deployment and maintenance costs by eliminating extensive parameter tuning. Furthermore, GlobeReady incorporates a unique confidence quantification system that flags low-certainty diagnostic outputs for clinician review, enhancing diagnostic reliability and safety. Its integrated case retrieval functionality facilitates rapid matching of similar cases directly from the feature library (without the need for re-training), thereby streamlining medical record tracing and supporting data annotation efforts within healthcare settings. This multifaceted system greatly boosts diagnostic accuracy and efficiency, while also laying a solid foundation for subsequent case analysis and clinical research. Overall, GlobeReady’s holistic approach, blending training-free deployment with advanced diagnostic tools, would empower eye care clinics to optimize clinical decision-making and streamline processes across applications such as disease diagnosis, similar cases retrieval, and data annotation.

Recently, several foundation models, such as UNI [24] and PLIP [25] for pathology images, RETFound [8] and VisionFM [9] for ophthalmic images, demonstrated promising performance in diverse downstream tasks. Different from RETFound [8] and VisionFM [9], GlobeReady employed two advanced pre-training methods, DINOv2 [13] and CLIP [14], were trained using massive synthetic data rich in ocular disease features together with over 475,000 ophthalmic image-text pairs. This endows GlobeReady with a strong capability to capture detailed features and inherent topological structures within ophthalmic imaging. It also robustly aligns visual features with semantic information, thereby enhancing the model’s accuracy in diagnosing ocular diseases. Moreover, adapting these models to specific clinical contexts typically requires retraining to accommodate varying diseases or feature distributions, which always demands significant technical intervention.

GlobeReady’s confidence-quantifiable ocular disease diagnosis further bolsters its reliability in complex clinical decision-making scenarios. Previous studies, such as UIOS [26] and FMUE25 [27], explored incorporating uncertainty evaluation into disease diagnosis to enhance the reliability of AI models. However, these approaches typically require retraining for specific tasks, which limits their ease of clinical adoption. Furthermore, although other studies [28, 29] have explored case-based medical image retrieval, these solutions typically function independently of diagnostic tools. In contrast, GlobeReady unifies diagnostic precision and case retrieval within a single, training-free platform. This allows for efficient clinical diagnosis across diverse ocular diseases and eliminates the need for specialized AI skills, thus offering a comprehensive solution that fosters ease of adoption in diverse clinical settings.

Despite these promising results, several limitations warrant further study. Although our dataset covers a broad spectrum of ophthalmic diseases, the inherent class imbalance, especially the underrepresentation of rare conditions, may constrain GlobeReady’s performance in downstream tasks. While we have augmented the dataset using a generative model to synthesize a large volume of ophthalmic images, the generation process lacked control over specific disease categories. To address this issue, a potential solution could involve exploring text-guided diffusion models [30–32] to generate category-specific samples, thereby enabling the construction of a more balanced and comprehensive dataset. While the confidence-quantifiable ocular disease diagnosis capability bolsters diagnostic safety, it may also flag some correctly classified cases, potentially increasing clinical workload. Achieving an optimal balance between sensitivity and operational efficiency will depend on refining the threshold calibration. Finally, with respect to the feature-based case retrieval function, the relatively low Top-1 accuracy highlights opportunities for improving the retrieval algorithm and broadening dataset coverage.

In conclusion, GlobeReady is an innovative, clinician-friendly ophthalmic AI platform that addresses key challenges in the application of foundation models in real-world clinical settings. It delivers high diagnostic accuracy and reliability across ophthalmic imaging modalities without requiring retraining or technical expertise. Its performance in mitigating domain shifts, coupled with high retrieval accuracy in real-world clinical evaluations, underscores its potential to bolster clinician efficiency, reduce reliance on model retraining, and streamline disease monitoring and management.

4 Methods

This study was approved by the Joint Shantou International Eye Center (JSIEC) Institutional Review Board and adhered to the principles of the Declaration of Helsinki. All fundus images used in this study were made de-identified before computational analysis and model development.

4.1 Datasets for developing GlobeReady

We compiled a dataset comprising 382,527 CFPs and 105,921 OCT scans (Supplementary Table 13), which encompass over 400 ocular diseases sourced from 39 publicly available datasets, online resources, and literature, across multiple ethnicities and regions around the globe. Utilizing these ophthalmic images, we trained and used FundusGAN [33] to synthesize 38 million ophthalmic images (25 million CFPs and 13 million OCT scans) to enhance the diversity and scale of our pretraining data. Leveraging these synthesized images, we used DI-NOv2 [13], a self-supervised pretraining method to develop a foundation model that captures detailed features and inherent topological structures within ophthalmic imagery. Concurrently, we curated 475,845 ophthalmic image-text pairs [34] (374,424 CFP-text pairs, and 101,421 OCT-text pairs) from the collected datasets, and further pre-trained the model using the contrastive learning framework CLIP [14]. This multimodal pretraining strategy effectively aligns visual features with semantic information to enhance the model’s ability to accurately diagnose ocular diseases.

4.2 Data for ocular disease identification

To evaluate GlobeReady’s performance in diagnosing retinal diseases from CFPs, we compiled a JLHW11 dataset (Supplementary Table 14), which includes 19,478 CFPs representing 10 retinal disease categories and a normal condition. These CFPs were acquired from four ophthalmic centers: the Joint Shantou International Eye Center (using Zeiss VISUMCAM 200, Topcon 3D OCT-2000, Topcon DRI OCT Triton, and Topcon TRC-NW8 devices), Longchuan People’s Hospital (using Zeiss VISUCAM 200), Haifeng Pengpai Memorial Hospital (using Zeiss VISUMCAM 200), and Wuhan Aier Eye Hospital (using Topcon DRI OCT Triton). The dataset was randomly partitioned into a reference subset of 11,670 CFPs, serving as a comprehensive feature library to guide diagnosis, and a testing subset of 7,808 CFPs, used to evaluate GlobeReady’s performance in diagnosing ocular disease.

To assess GlobeReady’s performance in diagnosing ocular diseases from OCT images, we curated a JSIEC-OCT15 dataset, acquired using Topcon 3D OCT-2000 and Topcon DRI OCT Triton devices at the Joint Shantou International Eye Center. This dataset is independent from the JLHW11 dataset and comprises 102,893 OCT scans and encompasses 15 types of ophthalmic diseases (Supplementary Table 15), and was divided into a reference set of 59,590 OCT scans and a test set of 43,303 OCT scans. Detailed information on the different datasets is provided in Supplementary Table 16.

4.3 Data for local retrieval augmented ocular disease diagnosis

To evaluate the performance of local retrieval augmented ocular disease diagnosis based on CFPs, we further deployed GlobeReady to 7 centers across different regions around the world, including China, Singapore, the

UK, and Vietnam. In China, our evaluation included three centers: Guangxi Jingliang Eye Hospital, representing the southern region, Qingdao Central Hospital, representing the eastern region, and Puning People’s Hospital, representing the southeastern region, thereby ensuring diverse regional representation. Specifically, the GJEH dataset across 11 categories from Guangxi Jingliang Eye Hospital was acquired by NIDEK AFC-100 (Supplementary Table 17), which includes 1,788 CFPs employed for local feature extraction and 1,199 CFPs for performance evaluation. The QCH dataset of Qingdao Central Hospital was collected by the device of Canon CX-1 Digital Retinal Camera (Supplementary Table 18), including 1,548 CFPs (covering 4 categories of normal, AMD, DR, and glaucoma), where 926 CFPs were used for local feature augmentation and 622 CFPs were adopted for performance evaluation. The PNH dataset comprises 8,654 CFPs across 11 disease categories, acquired at Puning People’s Hospital using a Topcon TRC-NW8 camera (Supplementary Table 19). Of these, 5,188 CFPs were used to construct a local feature augmentation library, while the remaining 3,466 CFPs served as an independent test set to evaluate GlobeReady’s performance.

To test GlobeReady’s performance on other ethnic groups, we included the Singapore Epidemiology of Eye Diseases Study (SEED) [35] from Singapore and a DR screening dataset from the University of Liverpool, in the UK, referred to as UKDR. The CFPs in SEED were collected from three different ethnic groups (Malay, Indian, and Singapore), consisting of 4,319 CFPs and covering three major eye diseases, such as AMD, DR, and glaucoma. We used 3,451 CFPs for local feature augmentation and 868 CFPs for performance evaluation (Supplementary Table 20). The UKDR dataset, used for DR screening, originates from the UK and primarily consists of images from Caucasian individuals (Supplementary Table 21). In this data setting, 2,166 CFPs serve as the local reference subset for local feature augmentation, while 542 CFPs are utilized for performance evaluation.

To test our model’s performance in a low-resource setting, we deployed it in the Binh Dinh Eye Hospital in Vietnam (Supplementary Table 22), utilizing a dataset of 4,034 CFPs covering 10 ocular diseases and normal conditions. The dataset was divided into a reference subset for local feature extraction (3,223 CFPs) and a testing subset (811 CFPs) for performance evaluation.

Furthermore, we deployed the GlobeReady platform at Wuhan Aier Eye Hospital and the Joint Shantou International Eye Center to evaluate its performance in ocular disease diagnosis with local feature retrieval augmentation. The Wuhan Aier Eye Hospital dataset (WAEH-OCT13; Supplementary Table 23) comprises 5,161 OCT scans covering the same 13 ocular conditions as those in the JSIEC-OCT15 dataset. For this study, 2,478 scans were designated as the reference subset for local feature extraction, while the remaining 2,683 scans were used for performance evaluation. At the Joint Shantou International Eye Center, a dataset collected using the Zeiss Cirrus HD-OCT 5000 device was named Zeiss-OCT11. It contains 2,573 OCT scans, with 1,035 used for local feature augmentation and 1,538 for performance evaluation (Supplementary Table 24). Additional dataset details are provided in Supplementary Table 16.

4.4 Data for open set anomaly detection

We constructed the CFPOOD49 dataset (Supplementary Fig. 4a, Supplementary Table 16), comprising 7,257 CFPs from 49 OOD ocular disease categories that do not present in the JLHW11 reference subset, along with 1,066 low-quality CFPs deemed unsuitable for diagnosis. These images were collected from four ophthalmic centers (Joint Shantou International Eye Center, Longchuan People’s Hospital, Haifeng Pengpai Memorial Hospital, and Wuhan Aier Eye Hospital) using Zeiss VISUMCAM 200, Topcon DRI OCT Triton, and Topcon TRC-NW8 devices. Additionally, we collected 2,594 OCT images representing 13 OOD disease categories absent from the JSIEC-OCT15 dataset, along with 1,066 low-quality OCT scans, from the Joint Shantou International Eye Center using Topcon 3D OCT-2000 and Topcon DRI OCT Triton devices. These were used to construct an OCT-OOD13 dataset for evaluating GlobeReady’s performance detecting OOD cases in OCT images (Supplementary Fig. 5a, Supplementary Table 16).

4.5 Data for feature-based case retrieval

To evaluate GlobeReady’s feature-based case retrieval for CFPs, we used 168 CFPs covering 12 ocular diseases, collected from BDEH Hospital in Vietnam using Canon CR2 AF and Crystalvue NFC-600 devices, as query images to retrieve similar cases from the JLHW11, CFPOOD49 and CFP700K databases. The CFP700K database is a large-scale collection of 747,237 de-identified and unlabeled CFPs sourced from multiple medical centers across Mainland China, spanning multiple years and acquired using a variety of imaging devices. GlobeReady’s OCT retrieval performance was evaluated using 150 OCT images from the Joint Shantou International Eye Center (acquired with the Topcon DRI OCT Triton) as query images to search against 34,384 unlabeled OCT scans from Wuhan Aier Eye Hospital, also acquired with the Topcon DRI OCT Triton.

4.6 FundusGAN for synthesizing ophthalmic images

We employed an advanced generative model, FundusGAN [33], to synthesize an additional 38 million images (25 million CFPs and 13 million OCT images) from our globally collected datasets. FundusGAN [33] utilizes a feature pyramid network (FPN) to extract and integrate multi-scale features ranging from large anatomical structures to subtle pathological lesions. Moreover, it employs a modified StyleGAN-based generator with dilated convolutions to enhance anatomical fidelity and detail. These features contribute to its remarkable performance in ophthalmic image synthesis. These 38 million synthetic images were used to pre-train our GlobeReady as described below.

4.7 Self-supervised pretraining using the synthetic Data

We use a specific configuration of DINOv2 [13], an advanced self-supervised learning method that leverages a teacher-student framework, where the student network learns to mimic the stable and robust representations produced by an exponentially moving average teacher across various augmented views. This approach enables the model to capture rich semantic and structural information without relying on labelled data, leading to efficient feature extraction and excellent generalization. These advantages make DINOv2 highly effective for foundation model pre-training. In our implementation, we employed a large Vision Transformer (ViT-large) [36] with a patch size of 16×16 , 24 Transformer blocks, and an embedding vector size of 1,024 as the backbone of our GlobeReady.

4.8 Contrastive language-image pre-training using ophthalmic image-text pairs

Although DINOv2 enables the extraction of structural and semantic features from images without extensive manual annotation [13], its ability to capture fine-grained feature attributes can benefit from further enhancement. To maintain GlobeReady’s robust structural and semantic representation while bolstering its capacity to learn detailed, disease-specific features, we implemented an additional pre-training phase based on the contrastive learning paradigm exemplified by CLIP [14]. Specifically, we integrated the Vision Transformer (ViT) backbone, initially pretrained with DINOv2, with Low-Rank Adaptation (LoRA) within a CLIP-based image-text pre-training framework. LoRA is a parameter-efficient fine-tuning technique that introduces trainable low-rank matrices into fixed pre-trained models [37], enabling effective adaptation with minimal additional parameters. Details about LoRA are illustrated in Supplementary Fig. 9. This approach preserves the core representational power of the pretrained ViT in capturing the intricate structural and semantic features of ophthalmic images, while reducing computational overhead. We conducted this training on a meticulously curated dataset comprising 475,875 ophthalmic image-text pairs [37], which facilitated robust alignment between visual and textual representations.

Moreover, ophthalmic image descriptions present unique challenges compared to those of natural images due to the prevalence of specialized clinical terminology and the inclusion of multiple lesion signs or even complete descriptive sentences. To effectively capture these complex textual features, we adopted the BioClinicalBERT [38] model as our text encoder, which was pre-trained on large-scale medical texts in the MIMIC-III dataset, thereby leveraging domain-specific linguistic knowledge. Subsequently, we fine-tuned the model using a vision-language contrastive learning framework tailored to extract ophthalmic-specific textual features. This approach would enhance the semantic alignment between visual and textual modalities and bolster the overall performance of our disease diagnosis.

4.9 Clinician-friendly diagnostic without technical barriers

Rather than relying on a fixed classifier, GlobeReady extracts high-dimensional visual features from query images and retrieves the most semantically similar cases from a curated library of labelled fundus and OCT images. Diagnostic predictions would then be inferred from the labels of top-matched reference cases, enabling immediate applicability across a wide range of ocular conditions and two imaging modalities. This eliminates the programming overhead and resource burden typically required for AI model retraining.

4.10 Adaptive ocular disease diagnosis by local retrieval augmented GlobeReady

AI models deployed in healthcare frequently require retraining or fine-tuning when introduced to new clinical environments due to significant variations in imaging protocols, equipment specifications, patient demographics, and disease prevalence. Such domain shifts can markedly reduce model generalizability, complicating widespread clinical adoption. To overcome these challenges, GlobeReady employs an adaptive, training-free diagnostic approach inspired by retrieval-augmented generation (RAG) methodologies derived from large language models [15, 16]. Unlike conventional strategies that necessitate parameter updates or full retraining, GlobeReady

dynamically integrates local, site-specific information by augmenting its global feature reference library with newly extracted features from local fundus or OCT images. This local feature augmentation process is straightforward. Upon deployment at a new clinical site, GlobeReady processes local images data using our pretrained model. This generates local feature embeddings, which are seamlessly integrated into the global reference feature repository, creating a hybrid retrieval database customized to the local clinical context. During diagnostic inference, the query image feature would be matched against this comprehensive and hybrid data repository, and then retrieves clinically similar cases, drawing from both globally established and locally augmented examples. By leveraging retrieval-based adaptation instead of traditional model retraining, GlobeReady aims to address domain shifts without incurring additional retraining costs.

4.11 Bayesian-based confidence evaluation in GlobeReady

To further enhance ocular disease diagnostic reliability, we incorporated Bayesian deep learning [39] and a Monte Carlo dropout (MC-Drop) approach [40] with the GlobeReady model, dubbed Bayesian GlobeReady. Specifically, during inference, the dropout layers remain active, allowing the model to perform 100 stochastic forward passes for each sample in the reference dataset, thereby generating a distribution of feature embeddings that encapsulate inherent variability. For each test sample, GlobeReady calculates similarity scores against these embeddings to obtain 100 prediction results. The final diagnosis is determined by selecting the most consistent prediction across passes, while the degree of consistency is used as a confidence score. This enables reliable diagnosis and helps flag ambiguous or out-of-distribution cases for further clinical review. The approach provides a scalable and robust framework for reliable ocular disease diagnosis.

4.12 Calculation of the confidence threshold

Confidence threshold (θ) is employed to assess the reliability of the model’s diagnostic outputs. Specifically, if a sample’s confidence score above θ , its diagnostic result is deemed reliable; conversely, if the score falls below θ , the result is considered unreliable and flagged for further review by an ophthalmologist.

$$\mathbb{R} = \mathbb{I}(CScore \geq \theta), \quad (1)$$

where \mathbb{I} and CScore are the indicator function and confidence score, respectively. \mathbb{R} represents the reliability of the corresponding diagnosis result. This additional evaluation helps mitigate the risk of misdiagnosis or missed diagnoses, thereby enhancing the overall clinical reliability of the deployed model. In this study, to balance sensitivity and specificity in retinal disease diagnosis, we adopt Youden’s index J [41] to determine the confidence threshold θ^* based on the distribution of confidence scores in the test dataset:

$$J(\theta) = Sensitivity(\theta) + Specificity(\theta) - 1, \quad (2)$$

Finally, the confidence threshold θ^* is calculated by:

$$\theta^* = \arg \max_{\theta} (J(\theta)). \quad (3)$$

Here, $Sensitivity(\theta)$ represents the true positive rate and $Specificity(\theta)$ represents the true negative rate for predictions deemed reliable at the threshold θ , respectively. This method ensures that our confidence-based triaging strategy effectively maximizes diagnostic performance while minimizing clinical risk.

4.13 Questionnaire details for GlobeReady platform

To evaluate the usability and acceptability of the GlobeReady platform, we conducted a survey based on the SUS [17] and the unified theory of acceptance and use of technology (UTAUT) [42]. The questionnaire included 19 questions, 10 of which were based on the SUS to estimate usability, and the others measured effectiveness, helpfulness, ease of use, and satisfaction (Supplementary Questionnaire). All the questions followed a five-point Likert scale. For the SUS, the score of each question ranged from 0 to 4. The cumulative SUS score was calculated by multiplying the sum of the score of each question by 2.5, ranging from 0 to 100. For the other sections, the scores of negative questions were converted in the same direction as the positive questions, i.e., the scores ranged from 1 to 5.

A total of seven ophthalmologists from China and Singapore were invited to participate in the survey, including 5 residents and 2 retinal specialists, with 2 to 9 years of clinical experience. The URL of the GlobeReady platform was sent to the participants along with three instructional videos and written guidelines (Supplementary Guidelines). The guidelines and videos included instructions for all three functions: fundus disease diagnosis, confidence-quantifiable ocular disease diagnosis, and featured-based case retrieval. The participants can conduct inferences through their own images following the instructions. The questionnaire was integrated into the website and participants were asked to complete the questionnaire right after using the platform. The results of the questionnaire were stored in the backend system. The mean scores and standard deviations were calculated for each question.

5 Data availability

The publicly available datasets used for pre-training are available at the following links and references:

APTOS: <https://www.kaggle.com/c/aptos2019-blindness-detection>.

Cataract: <https://www.kaggle.com/datasets/jr2ngb/cataractdataset>.

DDR: <https://github.com/nkicsl/DDR-dataset>.

Diabetic Retinopathy Level Detection: <https://www.kaggle.com/datasets/arbethi/diabetic-retinopathy-level-detection>.

Diabetic Retinopathy Organized: <https://www.kaggle.com/datasets/dola1507108/diabetic-retinopathy-organized>.

DR15: https://www.kaggle.com/datasets/nawa393/dr15_test.

Messidor: <https://paperswithcode.com/dataset/messidor-1>.

MURED: <https://www.kaggle.com/datasets/abhirampolisetti/multi-label-retinal-disease-mured-dataset>.

Retina Dataset: <https://www.kaggle.com/datasets/jr2ngb/cataractdataset>.

Kaggle DR: <https://www.kaggle.com/c/diabetic-retinopathy-detection/data>.

ODIR5K: <https://www.kaggle.com/datasets/andrewmvd/ocular-disease-recognition-odir5k>.

SIC dataset: <https://www.kaggle.com/competitions/innovation-challenge-2019/data>. AliOCT2Fundus:

<https://2024.asiateleophth.org/big-data-competition>. Retinal Rocks: <https://www.retinarocks.org/image-gallery>. AI-Challenge 2018: <https://github.com/ShawnBIT/AI-Challenger-Retinal-Edema-Segmentation>. RETOUCH dataset: <https://paperswithcode.com/dataset/retouch>. AliChallenge: <https://2024.asiateleophth.org/big-data-competition>.

ACRIMA [43], BEH [44], DeepDRiD [45], DR1-2 [46], E-ophta [47], AIROGS [48], DeepEyeNet [49], FIVES [50], G1020 [51], Glaucoma dataset [52, 53], IDRiD [54], JICHI [55], REFUGE [56], ORIGA [57], PARAGUAY [58], EyePACS AirDoc [59], JSIEC [60], RFMid [61], BRSET [62], ORDRD [63], IMDOCT [64].

6 Supplementary file

Supplementary file can be available at: https://drive.google.com/file/d/1gRktQ9fqnpjY_YfuFAkSNI40HqfcccGx

References

1. J. D. Steinmetz, R. R. Bourne, P. S. Briant, S. R. Flaxman, H. R. Taylor, J. B. Jonas, A. A. Abdoli, W. A. Abrha, A. Abualhasan, E. G. Abu-Gharbieh *et al.*, “Causes of blindness and vision impairment in 2020 and trends over 30 years, and prevalence of avoidable blindness in relation to vision 2020: the right to sight: an analysis for the global burden of disease study,” *The Lancet Global Health*, vol. 9, no. 2, pp. e144–e160, 2021.
2. M. J. Burton, J. Ramke, A. P. Marques, R. R. Bourne, N. Congdon, I. Jones, B. A. A. Tong, S. Arunga, D. Bachani, C. Bascaran *et al.*, “The lancet global health commission on global eye health: vision beyond 2020,” *The Lancet Global Health*, vol. 9, no. 4, pp. e489–e551, 2021.
3. S. Nusinovici, T. H. Rim, H. Li, M. Yu, M. Deshmukh, T. C. Quek, G. Lee, C. C. Y. Chong, Q. Peng, C. C. Xue *et al.*, “Application of a deep-learning marker for morbidity and mortality prediction derived from retinal photographs: a cohort development and validation study,” *The lancet Healthy longevity*, vol. 5, no. 10, 2024.
4. K. Zhang, R. Zhou, E. Adhikarla, Z. Yan, Y. Liu, J. Yu, Z. Liu, X. Chen, B. D. Davison, H. Ren *et al.*, “A generalist vision–language foundation model for diverse biomedical tasks,” *Nature Medicine*, pp. 1–13, 2024.
5. L. Dai, L. Wu, H. Li, C. Cai, Q. Wu, H. Kong, R. Liu, X. Wang, X. Hou, Y. Liu *et al.*, “A deep learning system for detecting diabetic retinopathy across the disease spectrum,” *Nature communications*, vol. 12, no. 1, p. 3242, 2021.
6. Y. Peng, W. Zhu, Z. Chen, M. Wang, L. Geng, K. Yu, Y. Zhou, T. Wang, D. Xiang, F. Chen *et al.*, “Automatic staging for retinopathy of prematurity with deep feature fusion and ordinal classification strategy,” *IEEE transactions on medical imaging*, vol. 40, no. 7, pp. 1750–1762, 2021.
7. A. Elsayy, T. D. Keenan, Q. Chen, A. T. Thavikulwat, S. Bhandari, T. C. Quek, J. H. L. Goh, Y.-C. Tham, C.-Y. Cheng, E. Y. Chew *et al.*, “A deep network deepopacitynet for detection of cataracts from color fundus photographs,” *Communications Medicine*, vol. 3, no. 1, p. 184, 2023.
8. Y. Zhou, M. A. Chia, S. K. Wagner, M. S. Ayhan, D. J. Williamson, R. R. Struyven, T. Liu, M. Xu, M. G. Lozano, P. Woodward-Court *et al.*, “A foundation model for generalizable disease detection from retinal images,” *Nature*, vol. 622, no. 7981, pp. 156–163, 2023.
9. J. Qiu, J. Wu, H. Wei, P. Shi, M. Zhang, Y. Sun, L. Li, H. Liu, H. Liu, S. Hou *et al.*, “Visionfm: a multi-modal multi-task vision foundation model for generalist ophthalmic artificial intelligence,” *arXiv preprint arXiv:2310.04992*, 2023.
10. A. Esteva, A. Robicquet, B. Ramsundar, V. Kuleshov, M. DePristo, K. Chou, C. Cui, G. Corrado, S. Thrun, and J. Dean, “A guide to deep learning in healthcare,” *Nature medicine*, vol. 25, no. 1, pp. 24–29, 2019.
11. R. Bommasani, D. A. Hudson, E. Adeli, R. Altman, S. Arora, S. von Arx, M. S. Bernstein, J. Bohg, A. Bosselut, E. Brunskill *et al.*, “On the opportunities and risks of foundation models,” *arXiv preprint arXiv:2108.07258*, 2021.

12. W. F. Wiggins and A. S. Tejani, "On the opportunities and risks of foundation models for natural language processing in radiology," *Radiology: Artificial Intelligence*, vol. 4, no. 4, p. e220119, 2022.
13. M. Oquab, T. Darcet, T. Moutakanni, H. Vo, M. Szafraniec, V. Khalidov, P. Fernandez, D. Haziza, F. Massa, A. El-Nouby *et al.*, "Dinov2: Learning robust visual features without supervision," *arXiv preprint arXiv:2304.07193*, 2023.
14. A. Radford, J. W. Kim, C. Hallacy, A. Ramesh, G. Goh, S. Agarwal, G. Sastry, A. Askell, P. Mishkin, J. Clark *et al.*, "Learning transferable visual models from natural language supervision," in *International conference on machine learning*. PmLR, 2021, pp. 8748–8763.
15. P. Lewis, E. Perez, A. Piktus, F. Petroni, V. Karpukhin, N. Goyal, H. Kuttler, M. Lewis, W.-t. Yih, T. Rocktaschel *et al.*, "Retrieval-augmented generation for knowledge-intensive nlp tasks," *Advances in neural information processing systems*, vol. 33, pp. 9459–9474, 2020.
16. X. Ma, Y. Gong, P. He, H. Zhao, and N. Duan, "Query rewriting in retrieval-augmented large language models," in *Proceedings of the 2023 Conference on Empirical Methods in Natural Language Processing*, 2023, pp. 5303–5315.
17. P. W. Jordan, B. Thomas, I. L. McClelland, and B. Weerdmeester, *Usability evaluation in industry*. CRC press, 1996.
18. V. Venkatesh, M. G. Morris, G. B. Davis, and F. D. Davis, "User acceptance of information technology: Toward a unified view," *MIS quarterly*, pp. 425–478, 2003.
19. S. Gur, A. Ali, and L. Wolf, "Visualization of supervised and self-supervised neural networks via attribution guided factorization," in *Proceedings of the AAAI conference on artificial intelligence*, vol. 35, no. 13, 2021, pp. 11 545–11 554.
20. D. Milad, F. Antaki, D. Mikhail, A. Farah, J. El-Khoury, S. Touma, G. M. Durr, T. Nayman, C. Playout, P. A. Keane *et al.*, "Code-free deep learning glaucoma detection on color fundus images," *Ophthalmology Science*, vol. 5, no. 4, p. 100721, 2025.
21. S. K. Wagner, B. Liefers, M. Radia, G. Zhang, R. Struyven, L. Faes, J. Than, S. Balal, C. Hennings, C. Kilduff *et al.*, "Development and international validation of custom-engineered and code-free deep-learning models for detection of plus disease in retinopathy of prematurity: a retrospective study," *The Lancet Digital Health*, vol. 5, no. 6, pp. e340–e349, 2023.
22. E. Bisong *et al.*, *Building machine learning and deep learning models on Google cloud platform*. Springer, 2019.
23. J. Barnes, *Microsoft Azure essentials Azure machine learning*. Microsoft Press, 2015.
24. R. J. Chen, T. Ding, M. Y. Lu, D. F. Williamson, G. Jaume, A. H. Song, B. Chen, A. Zhang, D. Shao, M. Shaban *et al.*, "Towards a general-purpose foundation model for computational pathology," *Nature Medicine*, vol. 30, no. 3, pp. 850–862, 2024.
25. Z. Huang, F. Bianchi, M. Yuksekgonul, T. J. Montine, and J. Zou, "A visual–language foundation model for pathology image analysis using medical twitter," *Nature medicine*, vol. 29, no. 9, pp. 2307–2316, 2023.
26. M. Wang, T. Lin, L. Wang, A. Lin, K. Zou, X. Xu, Y. Zhou, Y. Peng, Q. Meng, Y. Qian *et al.*, "Uncertainty-inspired open set learning for retinal anomaly identification," *Nature Communications*, vol. 14, no. 1, p. 6757, 2023.
27. Y. Peng, A. Lin, M. Wang, T. Lin, L. Liu, J. Wu, K. Zou, T. Shi, L. Feng, Z. Liang *et al.*, "Enhancing ai reliability: A foundation model with uncertainty estimation for optical coherence tomography-based retinal disease diagnosis," *Cell Reports Medicine*, vol. 6, no. 1, 2025.
28. J. Fang, H. Fu, and J. Liu, "Deep triplet hashing network for case-based medical image retrieval," *Medical image analysis*, vol. 69, p. 101981, 2021.
29. G. Quellec, M. Lamard, G. Cazuguel, L. Bekri, W. Daccache, C. Roux, and B. Cochener, "Automated assessment of diabetic retinopathy severity using content-based image retrieval in multimodal fundus photographs," *Investigative ophthalmology and visual science*, vol. 52, no. 11, pp. 8342–8348, 2011.
30. A. Ramesh, M. Pavlov, G. Goh, S. Gray, C. Voss, A. Radford, M. Chen, and I. Sutskever, "Zero-shot text-to-image generation," in *International conference on machine learning*. Pmlr, 2021, pp. 8821–8831.
31. A. Ramesh, P. Dhariwal, A. Nichol, C. Chu, and M. Chen, "Hierarchical text-conditional image generation with clip latents," *arXiv preprint arXiv:2204.06125*, vol. 1, no. 2, p. 3, 2022.
32. J. Betker, G. Goh, L. Jing, T. Brooks, J. Wang, L. Li, L. Ouyang, J. Zhuang, J. Lee, Y. Guo *et al.*, "Improving image generation with better captions," *Computer Science.*, vol. 2, no. 3, p. 8, 2023.
33. Q. Hou, M. Wang, P. Cao, Z. Ke, X. Liu, H. Fu, and O. R. Zaiane, "Fundusgan: A hierarchical feature-aware generative framework for high-fidelity fundus image generation," *arXiv preprint arXiv:2503.17831*, 2025.
34. M. Wang, T. Lin, A. Lin, K. Yu, Y. Peng, L. Wang, C. Chen, K. Zou, H. Liang, M. Chen *et al.*, "Common and rare fundus diseases identification using vision-language foundation model with knowledge of over 400 diseases," *arXiv preprint arXiv:2406.09317*, 2024.
35. S. Majithia, Y.-C. Tham, M.-L. Chee, S. Nusinovi, C. L. Teo, M.-L. Chee, S. Thakur, Z. D. Soh, N. Kumari, E. Lamoureux *et al.*, "Cohort profile: the singapore epidemiology of eye diseases study (seed)," *International journal of epidemiology*, vol. 50, no. 1, pp. 41–52, 2021.
36. A. Dosovitskiy, L. Beyer, A. Kolesnikov, D. Weissenborn, X. Zhai, T. Unterthiner, M. Dehghani, M. Minderer, G. Heigold, S. Gelly *et al.*, "An image is worth 16x16 words: Transformers for image recognition at scale," *arXiv preprint arXiv:2010.11929*, 2020.
37. E. J. Hu, Y. Shen, P. Wallis, Z. Allen-Zhu, Y. Li, S. Wang, L. Wang, W. Chen *et al.*, "Lora: Low-rank adaptation of large language models," *ICLR*, vol. 1, no. 2, p. 3, 2022.
38. E. Alsentzer, J. R. Murphy, W. Boag, W.-H. Weng, D. Jin, T. Naumann, and M. McDermott, "Publicly available clinical bert embeddings," *arXiv preprint arXiv:1904.03323*, 2019.
39. A. Kendall and Y. Gal, "What uncertainties do we need in bayesian deep learning for computer vision?" *Advances in neural information processing systems*, vol. 30, 2017.

40. Y. Gal and Z. Ghahramani, "Dropout as a bayesian approximation: Representing model uncertainty in deep learning," in *international conference on machine learning*. PMLR, 2016, pp. 1050–1059.
41. J. Luo and C. Xiong, "Youden index and associated cut-points for three ordinal diagnostic groups," *Communications in Statistics-Simulation and Computation*, vol. 42, no. 6, pp. 1213–1234, 2013.
42. A. Bangor, P. Kortum, and J. Miller, "Determining what individual sus scores mean: Adding an adjective rating scale," *Journal of usability studies*, vol. 4, no. 3, pp. 114–123, 2009.
43. A. Diaz-Pinto, S. Morales, V. Naranjo, T. Kohler, J. M. Mossi, and A. Navea, "Cnns for automatic glaucoma assessment using fundus images: an extensive validation," *Biomedical engineering online*, vol. 18, pp. 1–19, 2019.
44. M. T. Islam, S. T. Mashfu, A. Faisal, S. C. Siam, I. T. Naheen, and R. Khan, "Deep learning-based glaucoma detection with cropped optic cup and disc and blood vessel segmentation," *Ieee Access*, vol. 10, pp. 2828–2841, 2021.
45. R. Liu, X. Wang, Q. Wu, L. Dai, X. Fang, T. Yan, J. Son, S. Tang, J. Li, Z. Gao *et al.*, "Deepdrid: Diabetic retinopathy—grading and image quality estimation challenge," *Patterns*, vol. 3, no. 6, 2022.
46. R. Pires, H. F. Jelinek, J. Wainer, E. Valle, and A. Rocha, "Advancing bag-of-visual-words representations for lesion classification in retinal images," *PloS one*, vol. 9, no. 6, p. e96814, 2014.
47. E. Decenciere, G. Cazuguel, X. Zhang, G. Thibault, J.-C. Klein, F. Meyer, B. Marcotegui, G. Quellec, M. Lamard, R. Danno *et al.*, "Teleophtha: Machine learning and image processing methods for teleophthalmology," *Irbm*, vol. 34, no. 2, pp. 196–203, 2013.
48. C. De Vente, K. A. Vermeer, N. Jaccard, H. Wang, H. Sun, F. Khader, D. Truhn, T. Aimyshev, Y. Zhanibekuly, T.-D. Le *et al.*, "Airogs: artificial intelligence for robust glaucoma screening challenge," *IEEE transactions on medical imaging*, 2023.
49. J.-H. Huang, C.-H. H. Yang, F. Liu, M. Tian, Y.-C. Liu, T.-W. Wu, I. Lin, K. Wang, H. Morikawa, H. Chang *et al.*, "Deepopht: medical report generation for retinal images via deep models and visual explanation," in *Proceedings of the IEEE/CVF winter conference on applications of computer vision*, 2021, pp. 2442–2452.
50. K. Jin, X. Huang, J. Zhou, Y. Li, Y. Yan, Y. Sun, Q. Zhang, Y. Wang, and J. Ye, "Fives: A fundus image dataset for artificial intelligence based vessel segmentation," *Scientific Data*, vol. 9, no. 1, p. 475, 2022.
51. M. N. Bajwa, G. A. P. Singh, W. Neumeier, M. I. Malik, A. Dengel, and S. Ahmed, "G1020: A benchmark retinal fundus image dataset for computer-aided glaucoma detection," in *2020 International Joint Conference on Neural Networks (IJCNN)*. IEEE, 2020, pp. 1–7.
52. A. Singh, M. K. Dutta, M. ParthaSarathi, V. Uher, and R. Burget, "Image processing based automatic diagnosis of glaucoma using wavelet features of segmented optic disc from fundus image," *Computer methods and programs in biomedicine*, vol. 124, pp. 108–120, 2016.
53. A. Issac, M. P. Sarathi, and M. K. Dutta, "An adaptive threshold based image processing technique for improved glaucoma detection and classification," *Computer methods and programs in biomedicine*, vol. 122, no. 2, pp. 229–244, 2015.
54. P. Porwal, S. Pachade, M. Kokare, G. Deshmukh, J. Son, W. Bae, L. Liu, J. Wang, X. Liu, L. Gao *et al.*, "Idrid: Diabetic retinopathy—segmentation and grading challenge," *Medical image analysis*, vol. 59, p. 101561, 2020.
55. H. Takahashi, H. Tampo, Y. Arai, Y. Inoue, and H. Kawashima, "Applying artificial intelligence to disease staging: Deep learning for improved staging of diabetic retinopathy," *PloS one*, vol. 12, no. 6, p. e0179790, 2017.
56. J. I. Orlando, H. Fu, J. B. Breda, K. Van Keer, D. R. Bathula, A. Diaz-Pinto, R. Fang, P.-A. Heng, J. Kim, J. Lee *et al.*, "Refuge challenge: A unified framework for evaluating automated methods for glaucoma assessment from fundus photographs," *Medical image analysis*, vol. 59, p. 101570, 2020.
57. Z. Zhang, F. S. Yin, J. Liu, W. K. Wong, N. M. Tan, B. H. Lee, J. Cheng, and T. Y. Wong, "Origa-light: An online retinal fundus image database for glaucoma analysis and research," in *2010 Annual international conference of the IEEE engineering in medicine and biology*. IEEE, 2010, pp. 3065–3068.
58. V. E. C. Benitez, I. C. Matto, J. C. M. Roman, J. L. V. Noguera, M. Garcia-Torres, J. Ayala, D. P. Pinto-Roa, P. E. Gardel-Sotomayor, J. Facon, and S. A. Grillo, "Dataset from fundus images for the study of diabetic retinopathy," *Data in brief*, vol. 36, p. 107068, 2021.
59. L. Ju, X. Wang, L. Wang, D. Mahapatra, X. Zhao, Q. Zhou, T. Liu, and Z. Ge, "Improving medical images classification with label noise using dual-uncertainty estimation," *IEEE transactions on medical imaging*, vol. 41, no. 6, pp. 1533–1546, 2022.
60. L.-P. Cen, J. Ji, J.-W. Lin, S.-T. Ju, H.-J. Lin, T.-P. Li, Y. Wang, J.-F. Yang, Y.-F. Liu, S. Tan *et al.*, "Automatic detection of 39 fundus diseases and conditions in retinal photographs using deep neural networks," *Nature communications*, vol. 12, no. 1, p. 4828, 2021.
61. S. Pachade, P. Porwal, D. Thulkar, M. Kokare, G. Deshmukh, V. Sahasrabuddhe, L. Giancardo, G. Quellec, and F. Meriaudeau, "Retinal fundus multi-disease image dataset (rfmid): A dataset for multi-disease detection research," *Data*, vol. 6, no. 2, p. 14, 2021.
62. L. F. Nakayama, D. Restrepo, J. Matos, L. Z. Ribeiro, F. K. Malerbi, L. A. Celi, and C. S. Regatieri, "Brset: a brazilian multilabel ophthalmological dataset of retina fundus photos," *PLOS Digital Health*, vol. 3, no. 7, p. e0000454, 2024.
63. K. M. Adal, P. G. van Etten, J. P. Martinez, L. J. van Vliet, and K. A. Vermeer, "Accuracy assessment of intra- and intervisit fundus image registration for diabetic retinopathy screening," *Investigative ophthalmology and visual science*, vol. 56, no. 3, pp. 1805–1812, 2015.
64. D. S. Kermany, M. Goldbaum, W. Cai, C. C. Valentim, H. Liang, S. L. Baxter, A. McKeown, G. Yang, X. Wu, F. Yan *et al.*, "Identifying medical diagnoses and treatable diseases by image-based deep learning," *cell*, vol. 172, no. 5, pp. 1122–1131, 2018.